Supporting Information

Interfacial Electronic Coupling of Ultrathin Transition-Metal Hydroxides Nanosheets with Layered MXene as a New Prototype for Platinum-Like Hydrogen Evolution

Linlin Li, Deshuang Yu, Peng Li, Hongjiao Huang, Dengyu Xie, Chia-Ching Lin, Feng Hu, Han-Yi Chen, and Shengjie Peng*

Experimental section

Synthesis of $Ti_3C_2T_x$ ultrathin nanosheets

All chemicals and materials were used as received without further purification. $Ti_3C_2T_x$ MXene was synthesized by selective etching of Al from Ti_3AlC_2 using in situ HF-forming etchant. The etching solution was prepared by adding 2.0 g of lithium fluoride into 30 mL of 9 M hydrochloric acid followed by stirring for 5 min. Then, 2.0 g of Ti_3AlC_2 powder was slowly added into the above solution at 40 ℃ and stirred for 36 h. After that, the acidic suspension was washed with deionized (DI) water several times and centrifuged at 3500 rpm for 5 min until pH > 6. Finally, the obtained powders were dispersed in 250 mL of DI water and sonicated for 2 h under Ar flow, followed by centrifuging for 1 h at 3500 rpm. The resultant supernatant was decanted and collected. ($Ti_3C_2T_x$ MXene content ≈ 3 mg/mL).

Synthesis of TMHs@MXene

Typically, 1.164 g of $Co(NO_3)_2$ $6H_2O$ was dissolved in 25 mL of methanol to form solution A; then 0.6568 g of 2-methylimidazole was dissolved in a 25 mL of mixed solution (10 mL of MXene solution and 15mL of DI water) to form solution B. Subsequently, the solution B was poured into solution A under the ultrasonic condition. After aged for 1 h at room temperature, the resultant mixture was centrifuged and washed several time with DI water. Finally, the product was collected and freeze-dried, which was denoted as $Co(OH)_2$@MXene. For comparison, we performed controlled experiments with different MXene solutions (0 ml, 1 mL, 5 mL, and 25 mL) under other conditions unchanged, and the obtained products were marked as $Co(OH)_2$, $Co(OH)_2$@1MXene, $Co(OH)_2$@5MXene, and $Co(OH)_2$@25MXene, respectively. Notably, this protocol could be extended to prepare other transition metal hydroxides, such as

$Ni(OH)_2$@MXene and FeOOH@MXene, by simply modulation of chemical components in the precursors.

Synthesis of NiFe-LDH@NF

A piece of FeNi foam (NF) (1 ×2.5 cm^2) was washed with 2 M HCl, deionized water, and ethanol several times to ensure the removal of the surface oxides and organic species. The synthesis of NiFe-LDH@NF used a hydrothermal method. Firstly, the solution was prepared simply by dissolving 0.5 mM $Ni(NO_3)_2$ $6H_2O$, 0.5 mM $Fe(NO_3)_3$ $9H_2O$, and 5 mM $CO(NH_2)_2$ in 35 mL of deionized (DI) water with stirring for 15 min. Then, the as-prepared solution with a piece of NF was transferred into a 50 mL Teflon-lined autoclave, and kept at 120 ℃ for 12 h. After the autoclave cooling down to room temperature, the obtained NiFe-LDH@NF samples were washed with DI water and then dried in vacuum oven at 80 ℃ overnight.

Materials characterization

The crystal structure and morphology of the as-obtained samples were characterized by field-emission scanning electron microscope (FESEM; Regulus 8100) and X-ray diffraction (Bruker D8 Advance, Cu-Kα radiation, λ = 1.5418 Å). Transmission electron microscope (TEM) and energy-dispersive X-ray spectroscopy (EDX) mapping were obtained on FEI Tecnai G2 F20 electron microscope. The Brunauer-Emmetand-Teller (BET) surface area was performed using the instrument V-Sorb 2008P. X-ray photoelectron spectroscopy (XPS) was carried out on an Escalab 250Xi electron spectrometer (Thermo Fisher Scientific) equipped with mono-chromated Al Kα. The electron paramagnetic resonance (EPR) spectra were recorded using a Bruker EPR A300 spectrometer. The extended X-ray absorption fine structure (EXAFS) was measured at Taiwan Photon Source (TPS) beam line, 44A Quick-scanning X-ray absorption spectroscopy (XAS), in National Synchrotron Radiation Research Center (NSRRC), Hsinchu, Taiwan.

Electrochemical measurements

The electrochemical measurements were conducted in a three-electrode system using an electrochemical workstation (Autolab PGSTAT302, Eco Chemie, Netherlands). The working electrode was prepared by mixing the as-obtained catalyst with conductive agent (carbon black) and binder (Polyvinylidene fluoride, PVDF) in a ratio of 7:2:1 to form a homogeneous slurry. Then, the slurry was coated on Nickle Foam (NF) and dried at 80 ℃ in vacuum for 10 h. The loading mass of catalyst is around 1.0 mg cm^{-2}. The graphite rod and Ag/AgCl (Saturated KCl) electrode was served as counter electrode and reference electrode, respectively. And the measured potentials were converted to reversible hydrogen electrode (RHE) using the equation: E (vs. RHE) = E(Ag/AgCl) + 0.059 pH + 0.1979 V and the polarization curves were recorded at a scan rate of 5 mV s^{-1} with iR compensation in 1.0 M KOH. Electrochemically active surface areas were collected from Cyclic Voltammetry (CV) curves at non-Faraday area with different scan rates.

The HER stability of the catalysts was evaluated by chronopotentiometry method at a constant current density of 50 mA cm^{-2} for 65 h. Overall water splitting tests was carried out in a standard two-electrode system by using $Co(OH)_2$@MXene on NF as cathode and NiFe-LDH@NF as anode. Linear sweep voltammetry was carried out in 1.0 M KOH at 5 mV s^{-1} for the polarization curves. Chronopotentiometry was measured under a constant current density of 10 mA cm^{-2} for 100 h.

Computational details

Spin-polarized calculations were performed using the plane-wave pseudopotential method with the Vienna ab-initio Simulation Package (VASP) [1] based on the density functional theory (DFT). The electron-ion interactions were described by The Projector-augmented wave (PAW) pseudopotential[2]. The exchange-correlation interactions were treated by the generalized-gradient approximation (PBE/GGA) scheme[3]. The cut-off energy was set to 400 eV in all the calculations. The convergence thresholds were set as 1×10^{-6} eV/atom and 1×10^{-8} eV/atom in optimization and single point calculations, respectively.

The calculation models were constructed according to the micro-structures of composite catalyst. $Co(OH)_2$ (001) ribbon adsorbed on O-terminated Ti_3C_2 MXene (001) interface model was constructed to simulate the $Co(OH)_2$/MXene nanohybrids, as shown in Fig. 5(a). A vacuum thickness of 15 Å was set to avoid the interaction between periodic images. Grimme's semiempirical DFT-D scheme was used for dispersion correction between layers[4]. The Monkhorst-Pack grid of $6\times2\times1$ and $8\times4\times1$ were used to carry out for the intersurface optimization calculations and density of states (DOS) calculations, respectively.

The free energies of adsorbed states were defined as: $\Delta G = \Delta E + \Delta Ezpe - T\Delta S$, where ΔE is the adsorption energy of adsorbed H from DFT calculation. $\Delta Ezpe$ and ΔS are the difference in zero point energies and entropy during the reaction, respectively. Free energies calculation details can refer the previous reports.

[1] Kresse, G.; Furthmüller, *J. Comput. Mater. Sci.* 1996, 6, 15.

[2] Blöchl, P. E. *Phys. Rev. B* 1994, 50, 17953.

[3] Perdew, J. P.; W. Yue, *Phys. Rev. B* 1986, 33, 8800.

[4] Grimme, S. *J. Comput. Chem.* 2006, 27, 1787.

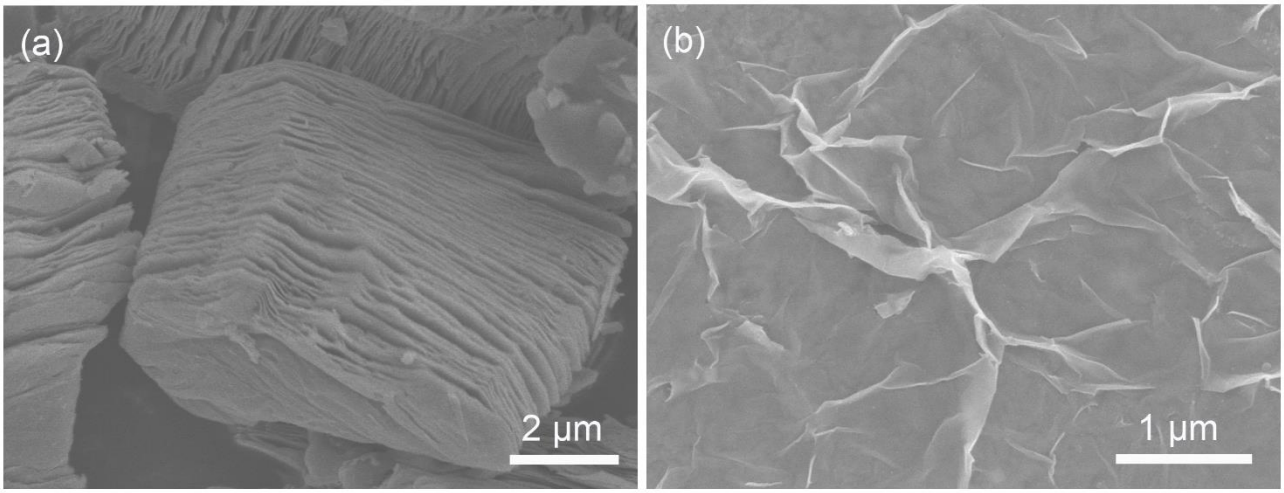

Fig.S1. SEM images of (a) an accordion-like $Ti_3C_2T_x$ MXene and (b) exfoliated ultrathin MXene nanosheets.

Fig.S1b shows the ultrathin MXene nanosheets with typical 2D layered strucutre, indicating the successful exfoliation of accordion-like $Ti_3C_2T_x$.

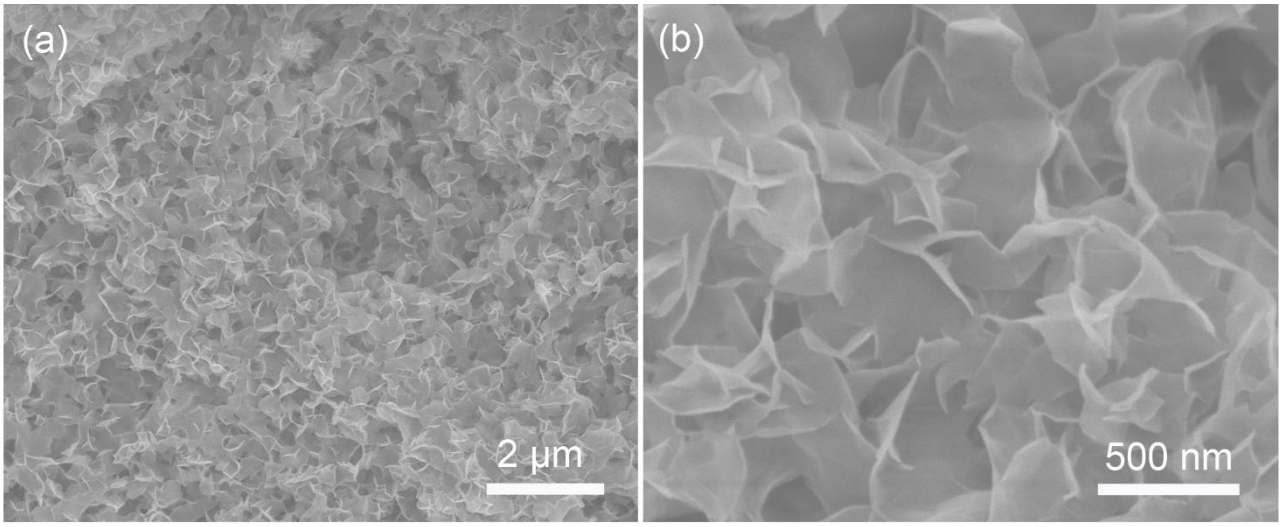

Fig.S2. (a and b) SEM images of bare $Co(OH)_2$ at different magnifications.

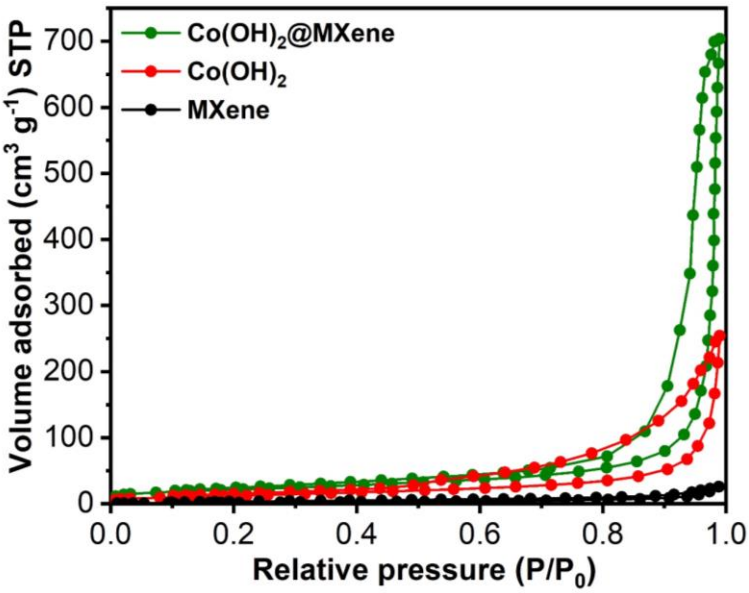

Fig.S3. The N_2 absorption and desorption isotherm of MXene, $Co(OH)_2$, and $Co(OH)_2$@MXene hybrids.

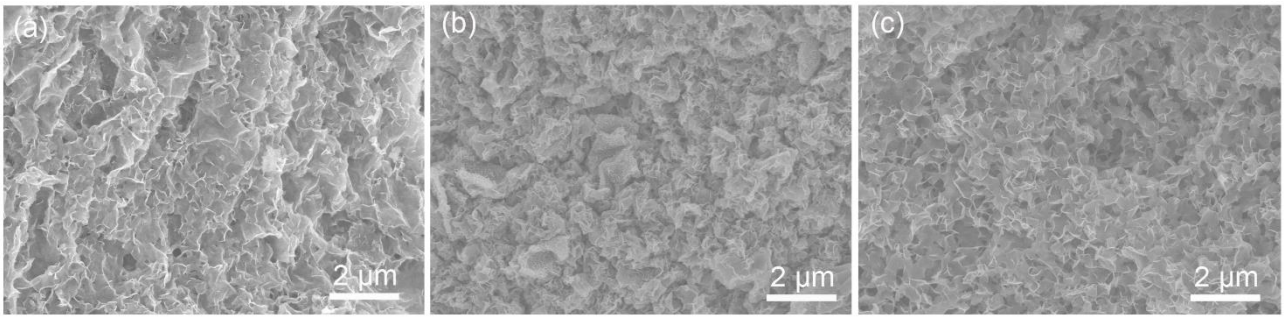

Fig.S4. SEM images of $Co(OH)_2$@MXene with different ratios (a) $Co(OH)_2$@1MXene, (b) $Co(OH)_2$@5MXene, and (c) $Co(OH)_2$@25MXene.

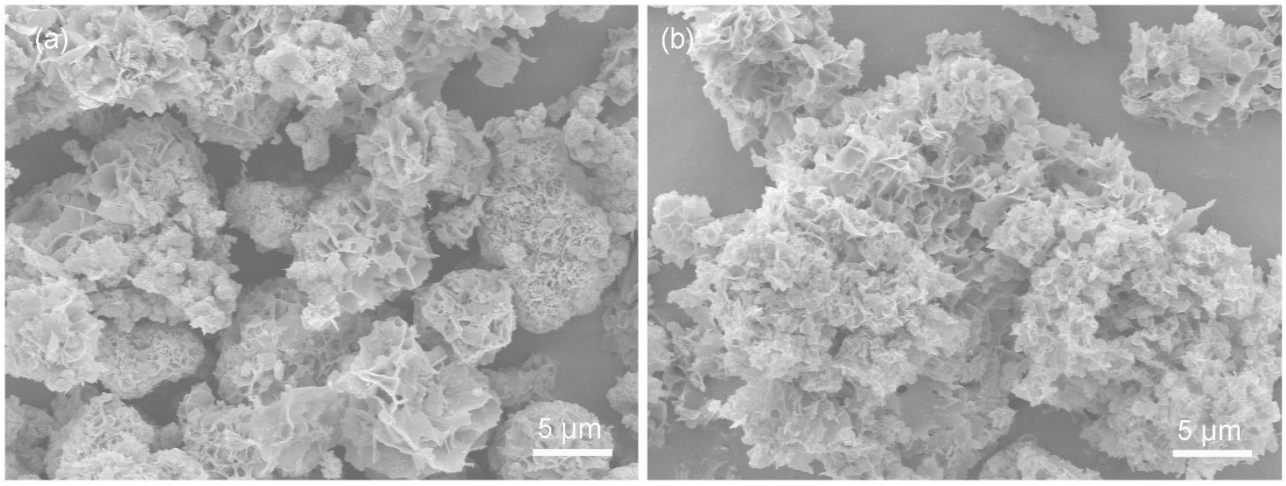

Fig.S5. SEM images of (a) $Ni(OH)_2$ and (b) $Ni(OH)_2$@MXene.

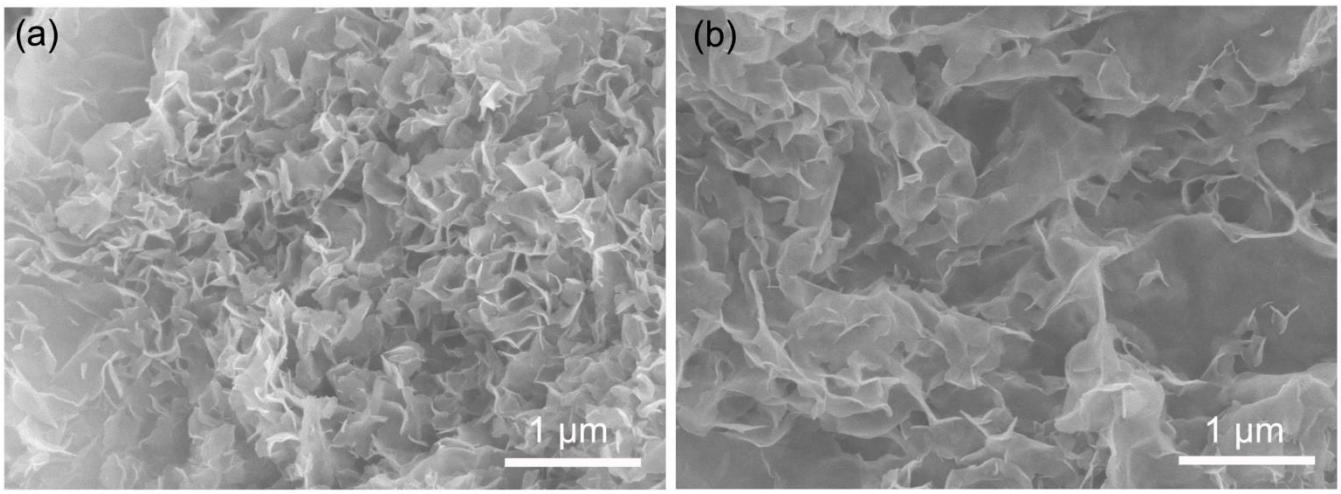

Fig.S6. SEM images of (a) FeOOH and (b) FeOOH@MXene.

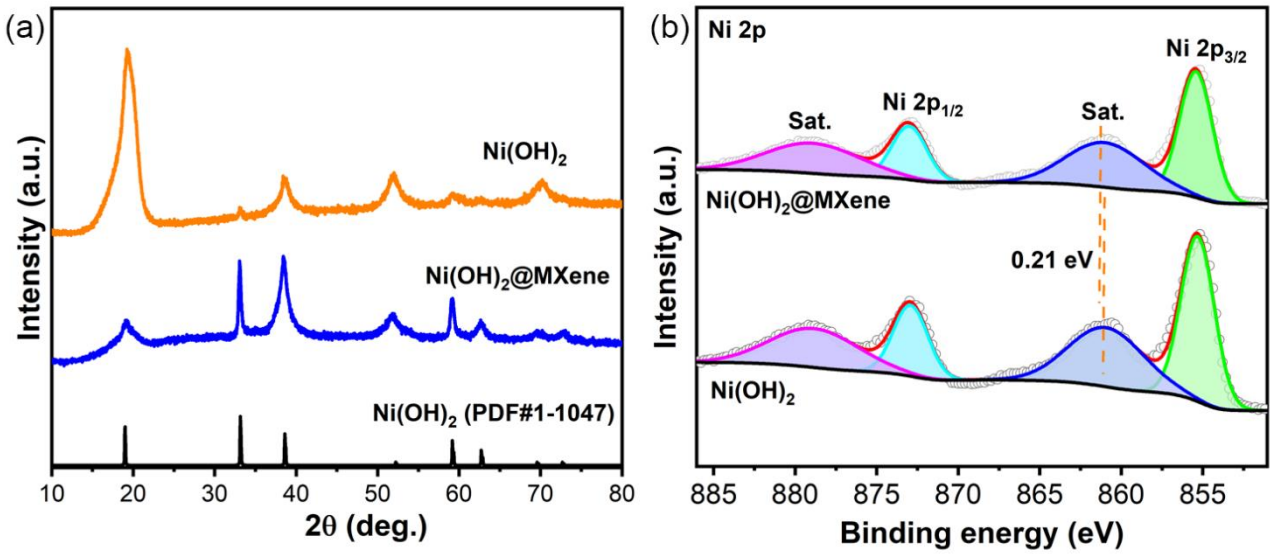

Fig.S7. (a) XRD and (b) XPS spectra of $Ni(OH)_2$ and $Ni(OH)_2$@MXene, respectively.

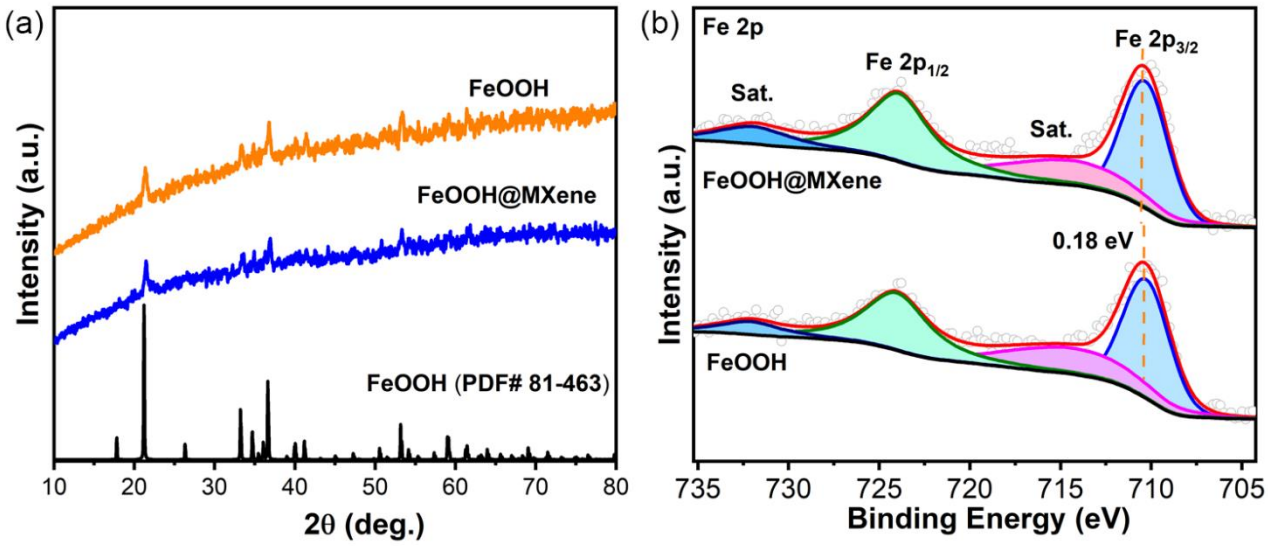

Fig.S8. (a) XRD and (b) XPS spectra of FeOOH and FeOOH@MXene, respectively.

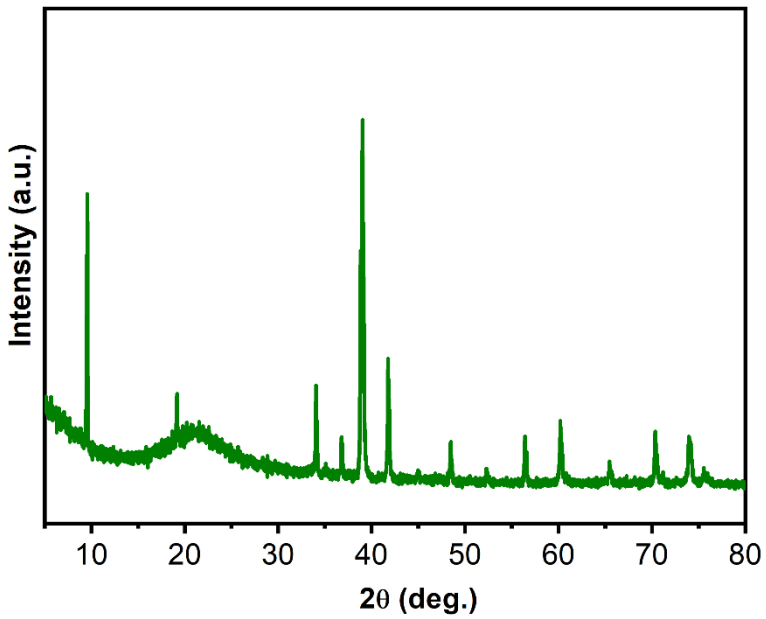

Fig.S9. XRD pattern of Ti_3AlC_2.

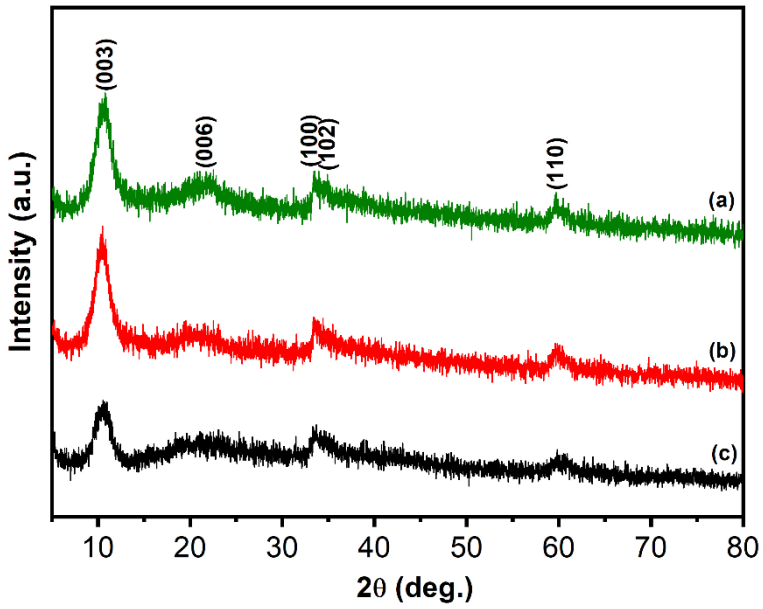

Fig.S10. XRD patterns of $Co(OH)_2$@MXene with different ratios (a) $Co(OH)_2$@1MXene, (b) $Co(OH)_2$@5MXene, and (c) $Co(OH)_2$@25MXene.

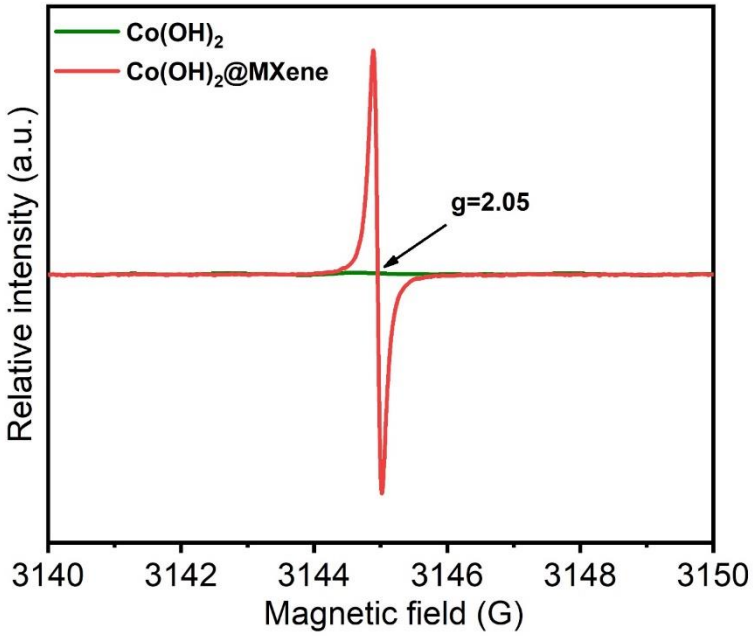

Fig.S11. EPR spectra of $Co(OH)_2$@MXene and $Co(OH)_2$.

EPR spectra were recorded to provide fingerprint evidence due to its sensitivity to unpaired electrons trapped by oxygen vacancies. A strong signal intensity at g = 2.05 was observed for $Co(OH)_2$@MXene, while $Co(OH)_2$ has a very weak signal, revealing a much higher concentration of oxygen vacancies in $Co(OH)_2$@MXene.

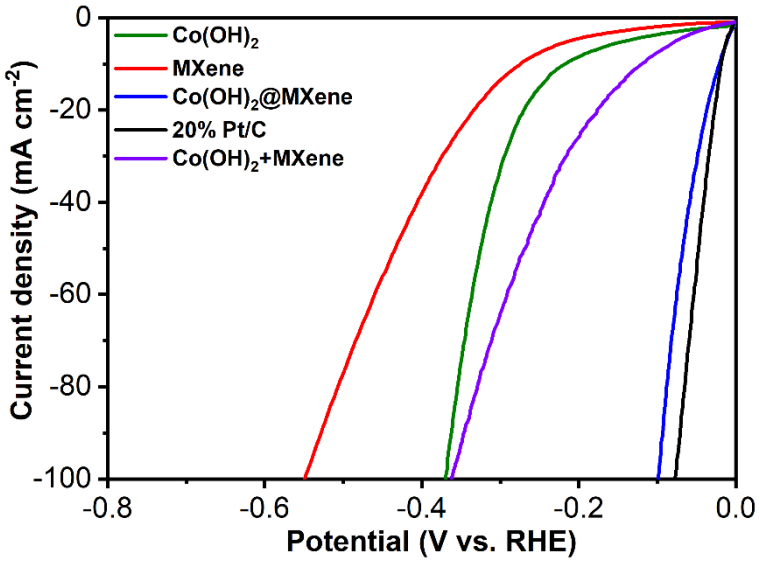

Fig.S12. HER Polarization curves of $Co(OH)_2$, MXene, $Co(OH)_2$@MXene, 20% Pt/C, and physical mixture ($Co(OH)_2$+MXene).

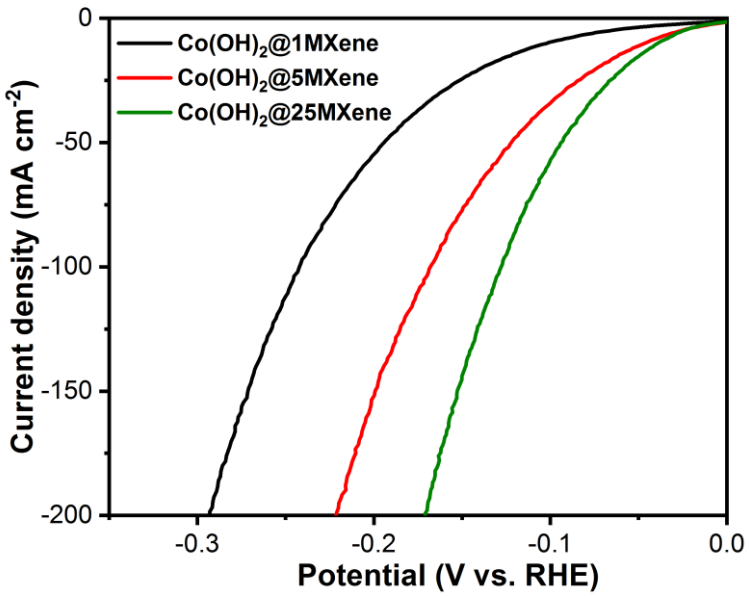

Fig.S13. HER Polarization curves of (a) $Co(OH)_2$@1MXene, (b) $Co(OH)_2$@5MXene, and (c) $Co(OH)_2$@25MXene.

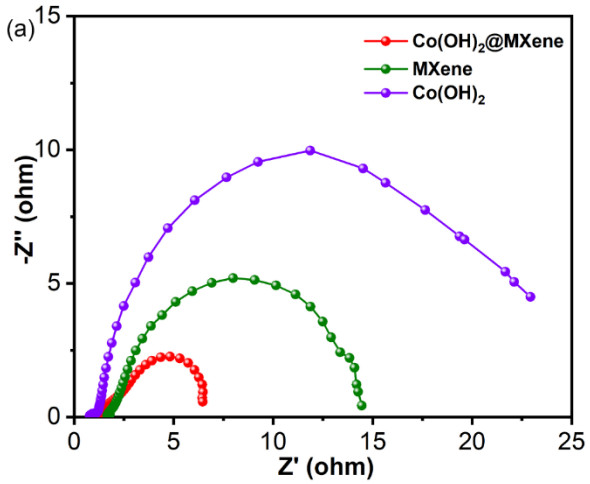

(b)

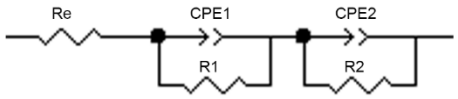

(c)

Impedance Parameter	Materials		
	$Co(OH)_2$@MXene	$Co(OH)_2$	MXene
R_e/Ω	1.3	0.9	0.7
R_2/Ω	4.1	11.3	20.9

Fig.S14. (a) Nyquist plots of $Co(OH)_2$, MXene, $Co(OH)_2$@MXene, respectively; (b) equivalent circuit model used to fit the experimental impedance spectra; (c) corresponding fitted impedance data obtained from Nyquist plots using the circuit in (b).

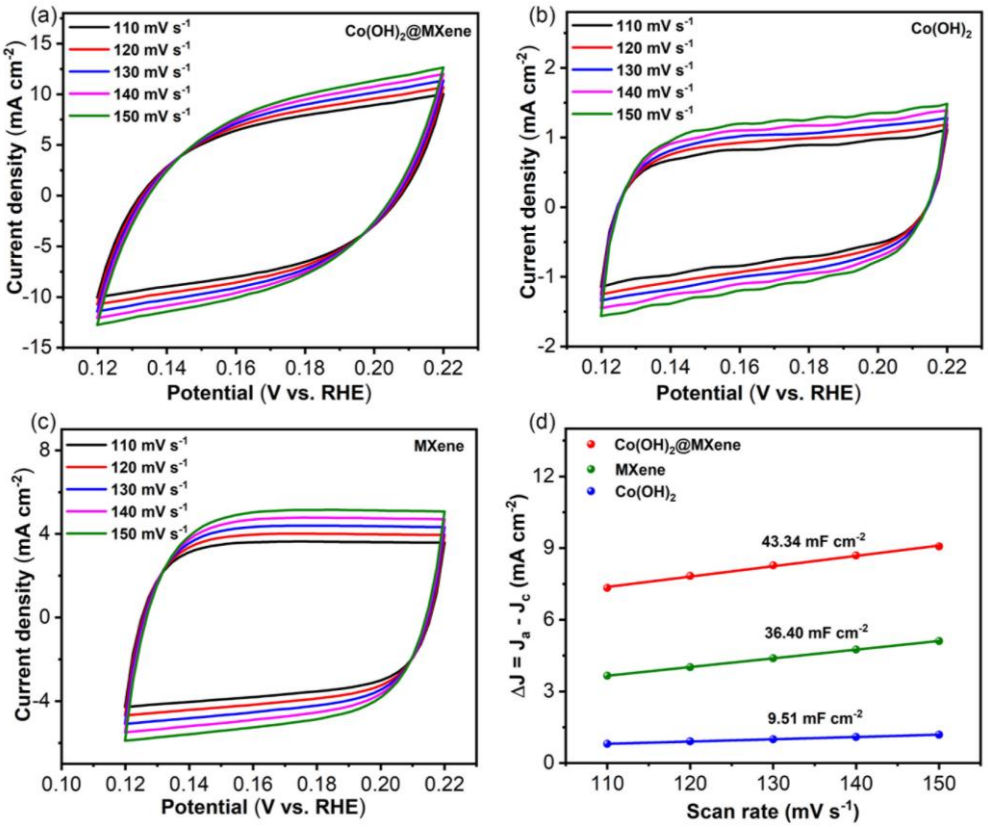

Fig.S15. (a-c) CV of $Co(OH)_2$@MXene, $Co(OH)_2$, and MXene at different scan rates in the voltage range of 0.12 to 0.22 V, respectively; (d) Double-layer capacitance (C_{dl}) of $Co(OH)_2$, MXene, $Co(OH)_2$@MXene (where ΔJ is the difference between anodic and cathodic current densities in CV curves at different scan rates in a non-Faradaic region).

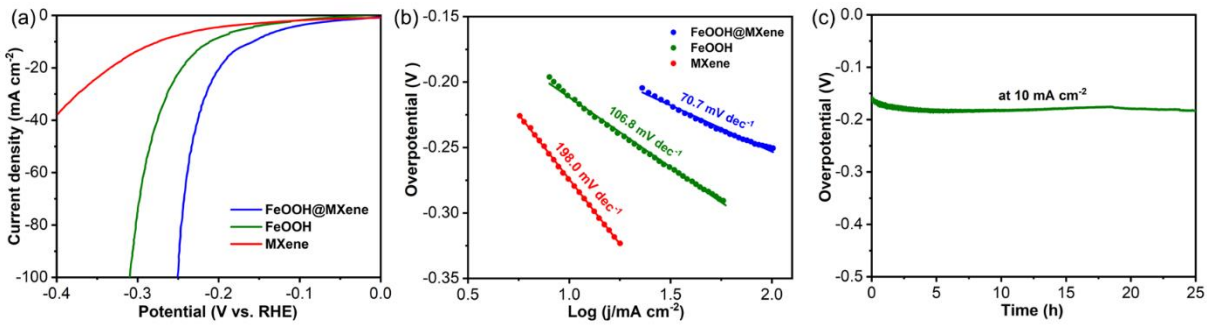

Fig.S16. (a) the HER Polarization curves; (b) corresponding Tafel plots of FeOOH, MXene, FeOOH@MXene in 1 M KOH; (c) long-term stability of FeOOH@MXene at current density of -10 mA cm^{-2}.

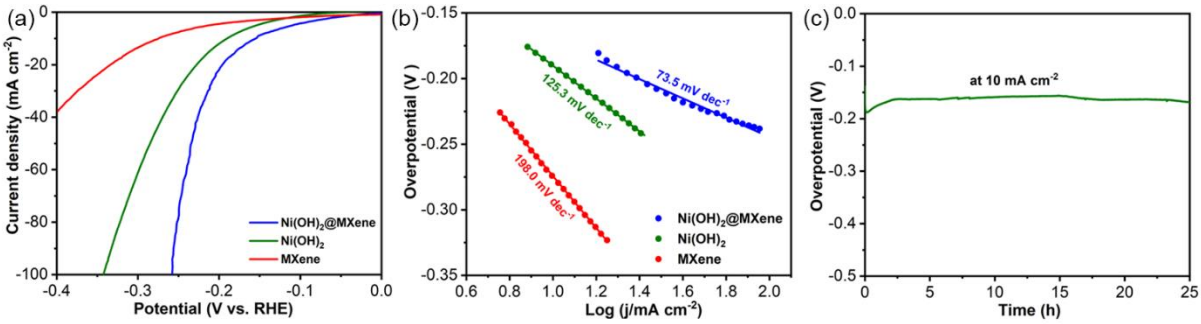

Fig.S17. (a) the HER Polarization curves; (b) corresponding Tafel plots of $Ni(OH)_2$, MXene, $Ni(OH)_2$@MXene in 1 M KOH; (c) long-term stability of $Ni(OH)_2$@MXene at current density of -10 mA cm^{-2}.

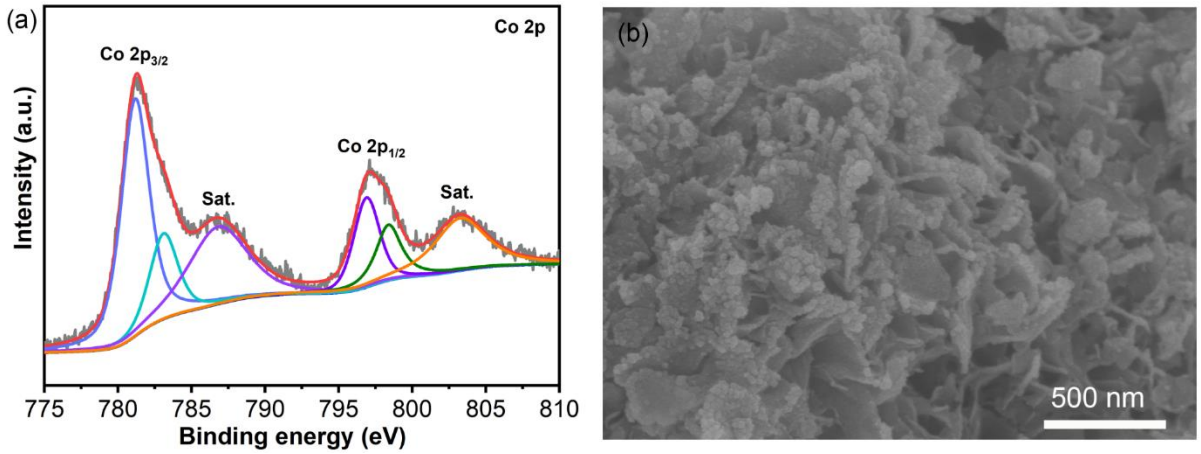

Fig.S18. (a) XPS spectra of Co2p and (b) SEM image of $Co(OH)_2$@MXene after HER cycling.

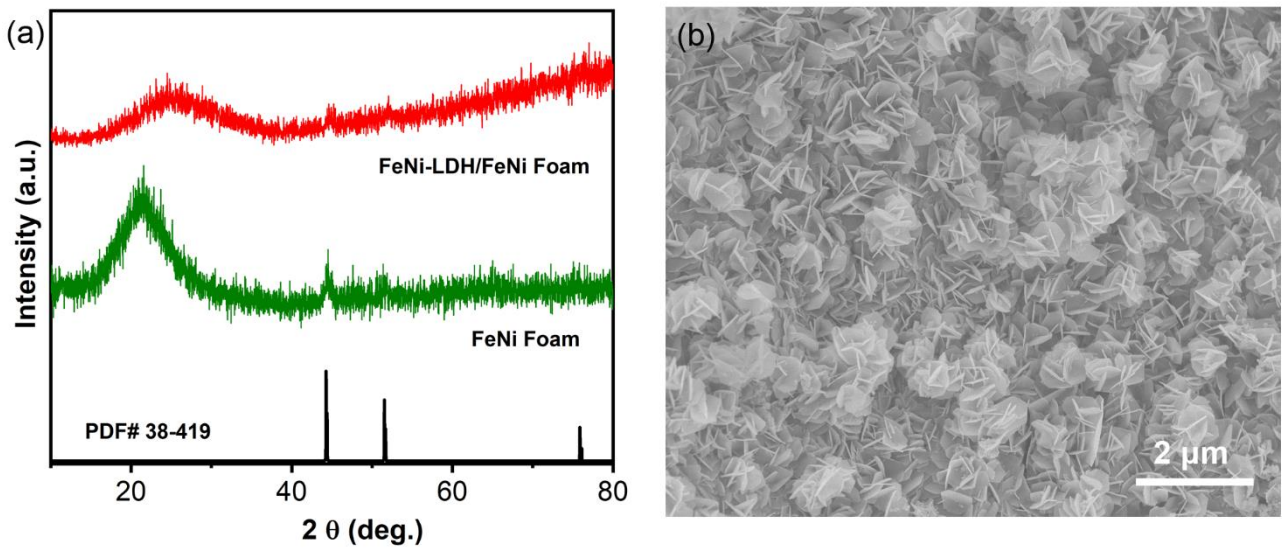

Fig.S19. (a) XRD and (b) SEM images of as-prepared FeNi-LDH.

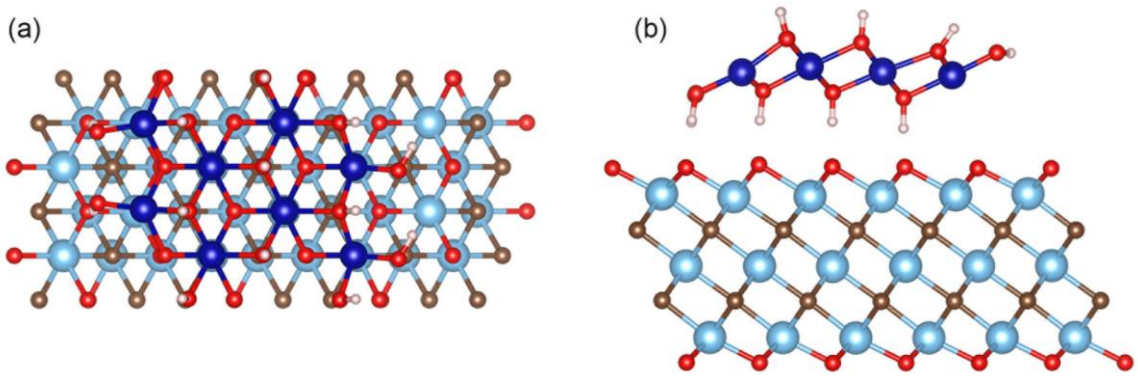

Fig.S20. (a) Top view and (b) side view structures of $Co(OH)_2$@MXene.

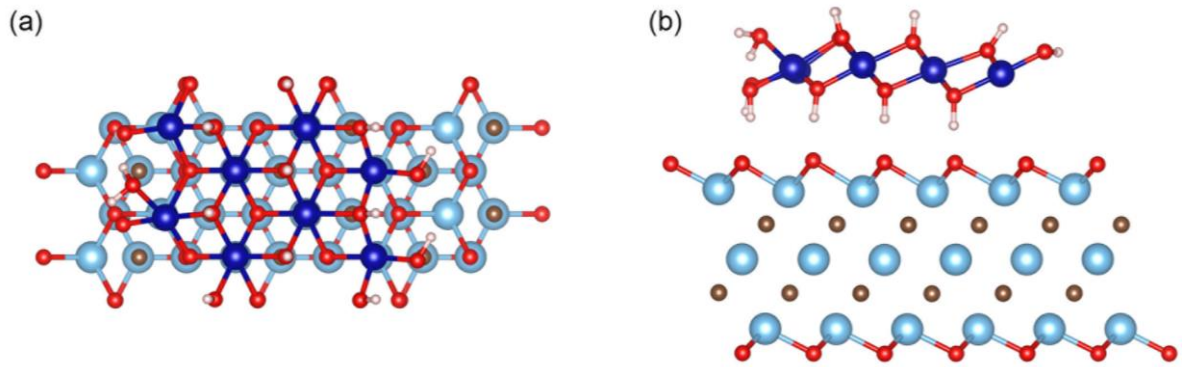

Fig.S21. (a) Top view and (b) side view structures of H_2O* adsorption on $Co(OH)_2$@MXene initially, respectively.

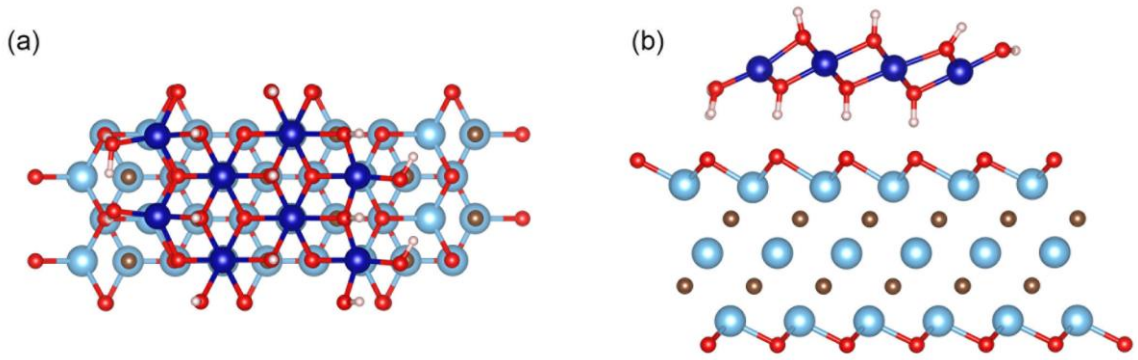

Fig.S22. (a) Top view and (b) side view structures of H* adsorption on $Co(OH)_2$@MXene initially, respectively.

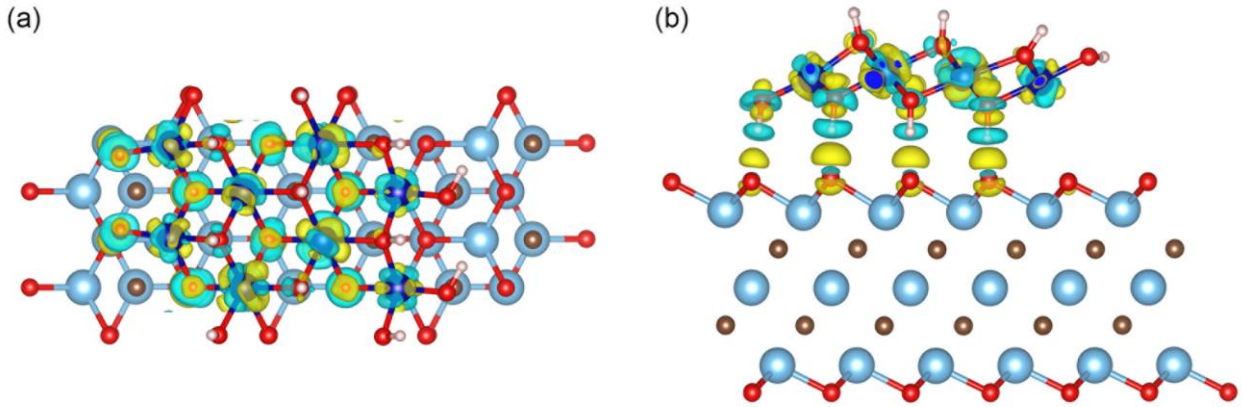

Fig.S23. (a) Top view and (b) side view of calculated charge density distribution differences of $Co(OH)_2$@MXene structures, respectively.

Table S1. CoK-edge EXAFS fitting of $Co(OH)_2$ and $Co(OH)_2$@MXene.

R is the bond distance; CN is coordination number; σ^2 is the Debye-Waller factor; E0 is adjustable "muffin-tin zero".

Sample	Path	CN	R(Å)	σ^2(Å^{-2})	E0(eV)
$Co(OH)_2$	Co-O	5.6	2.061	0.0179	-0.284
	Co-Co	6.0	3.097	0.0098	-0.284
$Co(OH)_2$@MXene	Co-O	5.9	2.069	0.0171	-0.422
	Co-Co	5.7	3.107	0.0105	-0.422

Table S2. Comparison of HER activity measured for $Co(OH)_2$@MXene with other representative reported HER oxides-based catalysts using 1.0 M KOH as electrolyte.

Sample	Loading amount (mg cm^{-2})	Current density (mA cm^{-2})	Overpotential (mV)	Tafel slope (mV dec^{-1})	References
$Co(OH)_2$@MXene	**1**	**10**	**21**	**31.7**	**This work**
C dopede NiO/Nickel foam	N.A.	10	27	36	Nat. Commun. 2020, 11, 1853.
$Ni(OH)_2/NiMoO_x$	1	10	36	38	Adv. Energy Mater. 2019, 9, 1902703.
$Ni_{11}(HPO_3)_8(OH)_6$	3	10	42	102	Energy Environ. Sci. 2018, 11, 1287.
$SrTi_{0.7}Ru_{0.3}O_{3-\delta}$	0.232	10	46	40	Nat. Commun. 2020, 11, 5657.
Ni-FeNP (Ni/γ-Fe_2O_3)	2.5	10	46	58	Nat. Commun. 2019, 10, 5599.
IFNOFs-45(FeF_2/Fe_2O_3)	0.2	10	47	31	Nat. Commun. 2018, 9, 1809.
Ni, Zn dual doped CoO NRs	0.486	10	53	47	Adv. Mater. 2019, 31, 1807771.
Fe-CoO NWs	0.248	10	53	65	J. Mater. Chem. A 2020, 8, 10831.
1T-MoS_2 QS/$Ni(OH)_2$	0.16	10	57	30	Adv. Funct. Mater. 2020, 30, 2000551.
DSO NiFe LDH	N.A.	10	59	62	Energy Environ. Sci. 2019, 12, 572.
MoO_3/Ni–NiO/Carbon cloth	N.A.	10	62	59	Adv. Mater. 2020, 32, 2003414.
ex-$MoSe_2$:$NiCl_2$/4-SWCNTs	0.8	10	64	114	Adv. Energy Mater. 2018, 8, 1801764.
$NiFeO_x$@NiCu	1	10	66	67.8	Adv. Mater. 2019, 31, 1806769.
V-CoP/a-CeO_2	0.8	10	68	48	Adv. Funct. Mater. 2020, 30, 1909618.
Co-doped CeO_2 NSs	4.2	10	70	N.A.	J. Am. Chem. Soc. 2020, 142, 6461.
CoMnO@CN superlattices	2	20	71	97	J. Am. Chem. Soc. 2015, 137, 14305.
Strained-CoO NRs	0.48	10	73	82	Nat. Commun. 2017, 8, 1509.
$MoS_2/Ni(OH)_2$	4.8	10	80	60	Nano Energy 2017, 37, 74.
$Co_3(OH)_2(HPO4)_2$	2	10	87	97	Adv. Funct. Mater. 2019, 29, 1808632.
$Se^{-}(NiCo)S_x/(OH)_x$	N.A.	10	87	103	Adv. Mater. 2018, 30, 1705538.
CoFeO@ black phosphorus	0.36	10	88	51	Angew.Chem.Int. Ed. 2020, 9, 21106.

MoS_2@$Co(OH)_2$	0.2	10	89	53	ACS Nano, 2018, 12, 4595.
VOOH-3Fe	0.2	10	90	38	Small 2019, 15, 1904688.
P-doped C_OMoO_4	N.A.	10	94	93	Adv. Sci. 2020, 7, 1903674.
CuS/$Ni(OH)_2$	0.286	10	95	104	Nano Energy 2018, 44, 7-14.
$NiCo_2O_4$ hollow microbuboids	1	10	100	50	Angew. Chem. Int. Ed. 2016, 55, 6290.
MoO_2-FeP	1.9	10	103	48	Adv. Mater. 2020, 32, 2000455.
CoFeZr oxide/NF	N.A.	10	104	119.3	Adv. Mater. 2019, 31, 1901439.
SCFP film	0.034	10	110	94	Adv. Mater. 2018, 30, 1804333.
NiFe LDH-NS@DG10	2	20	115	52	Adv. Mater. 2017, 29, 1700017.
N-doped $NiCo_2O_4$	~3.1	10	116	71	J. Mater. Chem. A, 2019, 7, 1468.
P-Co_3O_4	0.4	10	120	52	Energy & Environ. Sci. 2017, 10, 2563.
Ni-Laser (Ni/NiO)	N.A.	10	121	88	Nano Energy 2017, 35, 207.
2D MoS_2@$Co(OH)_2$	0.285	10	125	76	Adv. Mater. 2018, 30, 1801171.
R-NCO	2.5	10	135	52	J. Am. Chem. Soc. 2018, 140, 13644.
S-CoOx	2.1	10	136	80	Nano Energy 2020, 71, 104652.
Ni_3S_2/$NiWO_4$	5	10	136	112	Appl. Catal. B 2020, 274, 119120
PA-NiO/NF	N.A.	10	138	34	ACS Energy Lett. 2018, 3, 892.
mMoO_3	0.2	10	138	56	Adv. Energy Mater. 2016, 6, 1600528.
CuCoO-NWs	1.2	10	140	108	Adv. Funct. Mater. 2016, 26, 8555.
Co_3O_4-MTA	N.A.	10	158	98	Angew. Chem. Int. Ed. 2017, 56, 1324.
MoS_2/Co_3O_4	2	10	205	98	Appl. Catal. B: Environ. 2019, 248, 202.
A-PBCCF-H	N.A.	10	224	42	Nano Energy 2017, 32, 247.
Co^{II}Fe-ONC	1	10	240	76	Appl. Catal. B: Environ. 2019, 258, 117968.
$LiCo(H_2O)_2[BP_2O_8]$ ·H_2O	1	10	245	N.A.	Energy Environ. Sci. 2019, 12, 988.

CoO_x@CN	0.12	10	260	115	J. Am. Chem. Soc. 2015, 137, 2688.
Co_3O_4/C-QA	0.295	10	280	57	Adv. Funct. Mater. 2020, 30, 2000024.
2D $ZnCo_2O_4$	0.28	10	335	43	Small 2019, 15, 1904587.

Table S3. Comparison of overall water splitting performance in 1.0 M KOH for $Co(OH)_2$@MXene with other oxide-based electrocatalysts.

Sample	Current density (mA cm^{-2})	Potential (V)	References
$Co(OH)_2$@MXene‖NiFe-LDH	**10**	**1.46**	**This work**
Ni-FeNP (Ni/γ-Fe_2O_3)	10	1.47	Nat. Commun. 2019, 10, 5599.
DSO NiFe LDH	10	1.48	Energy Environ. Sci. 2019, 12, 572.
MoO_2-FeP	10	1.49	Adv. Mater. 2020, 32, 2000455.
MoO_2/NF	10	1.52	Adv. Mater. 2016, 28, 3785.
$LiCo(H_2O)_2[BP_2O_8]$ •H_2O	10	1.53	Energy Environ. Sci. 2019, 12, 988.
Fe-CoO NWs	10	1.53	J. Mater. Chem. A 2020, 8, 10831.
VOOH-0Fe	10	1.53	Small 2019, 15, 1904688.
RuO_2‖NiFeOx@NiCu	10	1.54	Adv. Mater. 2019, 31, 1806769.
$Co_3(OH)_2(HPO4)_2$	10	1.54	Adv. Funct. Mater. 2019, 29, 1808632.
CoO_x@CN	20	1.55	J. Am. Chem. Soc. 2015, 137, 2688.
PA-NiO	10	1.56	ACS Energy Lett. 2018, 3, 892.
V-CoP/a-CeO_2	10	1.56	Adv. Funct. Mater. 2020, 30, 1909618.
3D iron fluoride-oxide film	10	1.58	Nat. Commun. 2018, 9, 1809.
Ni/Ni(OH)2	10	1.59	Adv. Mater. 2020, 32, 1906915.
3D Se-$(NiCo)S_x/(OH)_x$	10	1.6	Adv. Mater. 2018, 30, 1705538.
CuCoO-NWs	10	1.61	Adv. Funct. Mater. 2016, 26, 8555.
R-NCO	10	1.61	J. Am. Chem. Soc. 2018, 140, 13644.
δ-FeOOH	10	1.61	Adv. Mater. 2018, 30, 1803144.
A-PBCCF-H	10	1.62	Nano Energy 2017, 32, 247.
$Ni_{11}(HPO_3)_8(OH)_6$	10	1.62	Energy Environ. Sci. 2018, 11, 1287.
CoFeZr oxide/NF	10	1.63	Adv. Mater. 2019, 31, 1901439.
Co_3O_4 nanorods	10	1.63	Angew. Chem. Int. Ed. 2017, 56, 1324.
CoFeZr oxides/NF	10	1.63	Adv. Mater. 2019, 31, 1901439.

S-CoO_x	10	1.63	Nano Energy 2020, 71, 104652.
Ni-Fe-O	10	1.64	Adv. Energy Mater. 2018, 8, 1701347.
S-$NiFe_2O_4$/NF	10	1.65	Nano Energy, 2017, 40, 264.
$Ni(OH)_2$/$NiMoO_x$	10	1.65	Adv. Energy Mater. 2019, 9, 1902703.
Ni-Laser (Ni/NiO)	10	1.66	Nano Energy 2017, 35, 207.
SCFP film	10	1.66	Adv. Mater. 2018, 30, 1804333.
$Co_5Mo_{1.0}O$ NSs@NF	10	1.68	Nano Energy, 2018, 45, 448.
Co^{II}Fe-ONC	10	1.71	Appl. Catal. B: Environ. 2019, 258, 117968.
Co_3O_4/C-QA	10	1.71	Adv. Funct. Mater. 2020, 30, 2000024.